Big Bang Nucleosynthesis

Big Bang Kernesyntese

Hans Brüner Dein
201706079

Master's Thesis in Cosmology
February 2024

Supervisor: Thomas Tram

Department of Physics and Astronomy
Aarhus University

Colophon

Big Bang Nucleosynthesis

— Big Bang Kernesyntese

Master's thesis by Hans. Written under supervision by Asc.Prof. Thomas Tram, Department of Physics and Astronomy, Aarhus University.

Typeset by the author with LaTeX and the memoir document class, using Linux Libertine and Linux Biolinum 11.0/13.6pt.

Printed at Aarhus University

Abstract (English)

Nucleosyntehesis is wack

Resumé (Dansk)

Kernesyntese er spøjs

Preface

This thesis concludes my Master's degree in/at .....

Contents

Introduction

This thesis is about nucleosynthesis

A brief history of early nucleosynthesis

A second after the Big Bang, the universe is at 10^10K. Though quite hot, this temperature is low enough that neutrons and protons can no longer maintain thermodynamics equilibrium, freezing their ratio at one to five. At approximately 200 seconds the universe has cooled sufficiently so that high energy photons can no longer destroy deuterium. This causes almost all neutrons to be use in the creation of deuterium, which is rapidly converted to helium. Due to the delay caused by deuterium, the temperature and density of the universe will be to low to create any more than trace amounts of heavier elements. And so a few minutes after it began, primordial nucleosynthesis ends. Barring radioactive decay, the abundance of the various elements will remain unchanged, until the first star appear 10^8 years later.

Chapter 1

BBN physics and cosmology

To understand the process of Big Bang nucleosynthesis, we must examine the intersection between Cosmology, thermodynamics, particle, and nuclear physics. Though this might seem daunting, it turns out that the unique conditions during this epoch allow for extensive simplifications of this otherwise monumental task. Throughout this section we use $\hbar = c = k_B = 1$.

1.1 Determining background parameters

1.1.1 Temperature and scale factor

BBN takes place after inflation while the universe is still radiation dominated. This can be described by the Friedman equation, which can be further simplified with the reasonable approximation, that both curvature and the cosmological constant are zero.

$$H^2 = \left(\frac{\dot{a}}{a}\right)^2 = \frac{8\pi G}{3}\rho_{tot}, \tag{1.1}$$

with ρ_{tot} referring to the total energy density of photons, leptons and baryons,

$$\rho_{tot} = \rho_\gamma + \rho_\nu + (\rho_{e^-} + \rho_{e^+}) + \rho_b. \tag{1.2}$$

(1.1) can be rearranged as a differential equation explicitly describing the time evolution of the scale factor.

$$\frac{da}{dt} = a\sqrt{\frac{8\pi G}{3}\rho_{tot}(T, a)} \tag{1.3}$$

To find an expression for the temperature evolution, we utilize energy conservation. We can consider the neutrinos as decoupled during BBN, and so the photon temperature will be determined by the remaining components. Since this point the universe is very much homogeneous and isotropic, we utilize the fluid equation for adiabatic expansion [10, (4.44)].

$$\dot{\rho_{set}} + 3\frac{\dot{a}}{a}(\rho_{set} + P_{set}) = 0 \tag{1.4}$$

With ρ_{set} being the density of none-decoupled components and P_{set} being their pressures.

$$\rho_{set} = \rho_\gamma + (\rho_{e^-} + \rho_{e^+}) + \rho_b \quad , \quad P_{set} = P_\gamma + (P_{e^-} + P_{e^+}) + P_b \tag{1.5}$$

Using the chain rule we can then set up a differential equation describing the time evolution of the photon temperature.

$$\frac{dT}{dt} = -3\frac{\dot{a}}{a}\frac{\rho_{set}(T,a) + P_{set}(T,a)}{\frac{d\rho_{set}(T,a)}{dT}} \tag{1.6}$$

1.1.2 Additional parameters

Most BBN codes are based on the original code by Wagoner described in section 2.1. These don't track the scale factor, but instead use the quantity h.

$$h = M_u \frac{n_b}{T_9^3} \tag{1.7}$$

M_u being atomic mass units, n_b the baryon number density, and T_9 the temperature in 10^9 Kelvin. This quantity was useful since it stays approximately constant throughout BBN, while being easy to directly convert to baryon density. However, with modern computers this numerical simplicity is inconsequential, and as such it is more instructive to track the scale factor. The electron chemical potential was also tracked by the Wagoner code and its successors. The main effect of this is ensuring a non-zero electron density after e^- e^+ annihilation. We can easily set this to 0, as the impact will be 3 orders of magnitude lower than the already miniscule impact of the baryon density.

Neutrino temperature?

1.2 Energy densities and pressure

In the very early universe most particles were in thermal equilibrium, and can be described by the rules of statistical physics. The average number of particles in a given state is governed by the Fermi-Dirac distribution for fermions, and the Bose-Einstein distribution for bosons.

$$\bar{n}_{FD} = \frac{1}{e^{(E-\mu)/T} + 1} \quad , \quad \bar{n}_{BE} = \frac{1}{e^{(E-\mu)/T} - 1} \tag{1.8}$$

With E being the total energy each particle in the state and μ the chemical potential. The number density can be found generally by integrating over all possible momentum states.

$$n(T) = \frac{g}{(2\pi)^3}\int_0^\infty \bar{n}(p,T)dp^3 = \frac{g}{2\pi^2}\int_0^\infty \bar{n}(p,T)p^2dp \tag{1.9}$$

With g being the degeneracy parameter. We can similarly find an expression for the energy density by multiplying the integrand by the relativistic energy $E^2 = m^2 + p^2$.

$$\rho(T) = \frac{g}{2\pi^2}\int_0^\infty \bar{n}(p,T)\sqrt{m^2+p^2}p^2dp \tag{1.10}$$

Pressure is defined as the force exerted per unit area. Consider a relativistic particle confined to a sphere of radius r. Whenever it collides with the surface, it will exert a force proportional to the change in momentum.

$$F = \frac{dp}{dt} = \frac{\Delta p}{\Delta t} \quad , \quad \Delta p = 2p\cos\theta, \tag{1.11}$$

with θ being the incident angle.

The time between collisions can be deduced based on the distance traveled.

$$\Delta t = \frac{L}{\mathrm{v}} = L\frac{\sqrt{m^2+p^2}}{p}, \tag{1.12}$$

with distance between collisions L and velocity v.

Next, consider the triangle created by the center of the sphere and two consecutive collision points. Using the law of cosines we can determine L.

$$r^2 = L^2 + r^2 + 2Lr\cos\theta \Rightarrow L = 2r\cos\theta \tag{1.13}$$

We can then determine the force and pressure exerted on the sphere by each particle.

$$F = \frac{p^2}{r\sqrt{m^2+p^2}} \quad , \quad P = \frac{p^2}{4\pi r^3\sqrt{m^2+p^2}} \tag{1.14}$$

Generalizing this for any volume, we get the integral for the total pressure of a relativistic gas.

$$PV = \frac{p^2}{3\sqrt{m^2+p^2}} \tag{1.15}$$

$$P(T) = \frac{g}{6\pi^2}\int_0^\infty \bar{n}(p,T)\frac{p^4}{\sqrt{m^2+p^2}}dp \tag{1.16}$$

Additionally, we see that the pressure of an ultra-relativistic gas follows a simple relation.

$$P(T) = \frac{\rho(T)}{3} \quad (\text{for } m \ll p) \tag{1.17}$$

1.2.1 Photons

Photons are massless bosons with 2 distinct polarizations for each momentum state. With $g = 2$, we use 1.10 to determine the energy density.

$$\rho_\gamma(T) = \int_0^\infty \frac{p^3}{\pi^2}\frac{1}{e^{p/T}-1}dp = \frac{T^4}{\pi^2}\int_0^\infty \frac{u^3}{e^u-1}du \tag{1.18}$$

This integral is a well know representation of the Riemann Zeta function [22, (25.5.1)].

$$\rho_\gamma(T) = \frac{T^4}{\pi^2}\Gamma(4)\zeta(4) = \frac{\pi^2}{15}T^4 \tag{1.19}$$

From this we can easily determine the temperature derivative and pressure.

$$\frac{d\rho_\gamma(T)}{dT} = \frac{4}{15}\pi^2T^3 \quad , \quad P_\gamma(T) = \frac{\rho_\gamma(T)}{3} \tag{1.20}$$

1.2.2 Neutrinos

For neutrinos $g = 2N_\nu$, to account for the different species and their antiparticles.

$$\rho_\nu(T_\nu) = N_\nu \int_0^\infty \frac{p^3}{\pi^2} \frac{1}{e^{p/T_\nu} + 1} dp = N_\nu \frac{T_\nu^4}{\pi^2} \int_0^\infty \frac{u^3}{e^u + 1} du \tag{1.21}$$

This is also an integral representation of the Riemann Zeta function [22, (25.5.3)].

$$\rho_\nu(T_\nu) = N_\nu \frac{T_\nu^4}{\pi^2} \Gamma(4)\zeta(4)(1 - 2^3) = N_\nu \frac{7}{8} \frac{\pi^2}{15} T_\nu^4 \tag{1.22}$$

The effective neutrino number is $N_\nu = 3.045$ to take into account distortions caused by non-instantaneous decoupling of the neutrinos as well as QED plasma effects [14].

Tracking the neutrino temperature separately is quite troublesome, luckily we don't have to. Since neutrinos decouple very early, the only significant change in their energy density will be due to the expansion of the universe. Therefore, we can approximate the later evolution using the scale factor.

$$\rho_\nu(t) = \frac{\rho_\nu(T_i)}{a(t)^4} \tag{1.23}$$

This does not take into account the small energy transfer from e^+ e^- annihilation due to incomplete decoupling of neutrinos. However, a fully consistent calculation of this effect is beyond both the scope and focus of this thesis, and will thus be omitted.

1.2.3 Electrons and positrons

Electrons and positrons unfortunately have mass, which makes solving for their density and pressure much more troublesome.

$$\rho_\pm(T) = \frac{1}{\pi^2} \int_0^\infty \frac{\sqrt{m^2 + p^2}}{e^{(E \pm \mu)/T} + 1} p^2 dp \tag{1.24}$$

$$P_\pm(T) = \frac{1}{3\pi^2} \int_0^\infty \frac{1}{e^{(E \pm \mu)/T} + 1} \frac{p^4}{\sqrt{m^2 + p^2}} dp \tag{1.25}$$

Inspired by the derivation of Chandrasekhar [1], we will solve these integrals by using the rapidity θ.

$$\sinh\theta = \frac{p}{m} \quad , \quad \cosh\theta = \frac{E}{m} \tag{1.26}$$

After a simple change of variable we get a much nicer form of the integrals.

$$\rho_\pm(T) = \frac{m^4}{\pi^2} \int_0^\infty \frac{\sinh^2\theta \cosh^2\theta}{e^{(m\cosh\theta \pm \mu)/T} + 1} d\theta \tag{1.27}$$

$$P_\pm(T) = \frac{m^4}{3\pi^2} \int_0^\infty \frac{\sinh^4\theta}{e^{(m\cosh\theta \pm \mu)/T} + 1} d\theta \tag{1.28}$$

Next, we start by considering the geometric series.

$$\frac{1}{1+x} = \sum_{n=0}^{\infty}(-1)^n x^n \quad , \quad \text{for } |x| < 1 \tag{1.29}$$

Multiplying both sides by x grants us the very useful expansion:

$$\frac{1}{x^{-1}+1} = \sum_{n=1}^{\infty}(-1)^{n+1} x^n \quad , \quad \text{for } |x| < 1 \tag{1.30}$$

Before and during BBN $(E \pm \mu)/T$ will be strictly positive, enabling $x = e^{-(E\pm\mu)/T}$.

$$\frac{1}{e^{(m\cosh\theta\pm\mu)/T}+1} = \sum_{n=1}^{n=\infty}(-1)^{n+1} e^{-n\frac{m}{T}\cosh\theta} e^{\mp n\frac{\mu}{T}} \tag{1.31}$$

The chemical potential does not depend on the rapidity, allowing us to get combined pressure of both electrons and positrons.

$$P_e(T) = P_- + P_+ = \frac{2m^4}{3\pi^2}\sum_{n=1}^{n=\infty}(-1)^{n+1}\cosh\left(n\frac{\mu}{T}\right)\int_0^{\infty} e^{-n\frac{m}{T}\cosh\theta}\sinh^4\theta d\theta \tag{1.32}$$

These terms are integral representations of modified Bessel functions [22, (10.32.8)].

$$\int_0^{\infty} e^{-z\cosh\theta}\sinh^4\theta d\theta = 4\frac{\Gamma(2+\frac{1}{2})}{\sqrt{\pi}z^2}K_2(z) = 3z^{-2}K_2(z) \tag{1.33}$$

With $z = n\frac{m}{T}$, we can get the total pressure expressed as a sum of modified Bessel functions.

$$P_e(T) = \frac{2m^2}{\pi^2}T^2\sum_{n=1}^{n=\infty}\frac{(-1)^{n+1}}{n^2}\cosh\left(n\frac{\mu}{T}\right)K_2\left(n\frac{m}{T}\right) \tag{1.34}$$

The energy density can be found by the same way, by first utilizing the identity $cosh^2 = sinh^2 + 1$, to get the energy density in terms of $\sinh\theta$.

$$\rho_e(T) = \rho_- + \rho_+ = \frac{2m^4}{\pi^2}\sum_{n=1}^{n=\infty}(-1)^{n+1}\cosh\left(n\frac{\mu}{T}\right)\int_0^{\infty} e^{-n\frac{m}{T}\cosh\theta}\left(\sinh^4\theta + \sinh^2\theta\right)d\theta \tag{1.35}$$

The $\sinh^4$ term is clearly the same as for the pressure up to a factor of 3. Comparing this to the results for massless particles, this term can be interpreted as the thermal energy of the electron gas. The second term also corresponds to a modified Bessel function, though of first rather than second order [22, (10.32.8)]. Combined this grants us the sum describing the total energy density of electrons and positrons.

$$\rho_e(T) = \frac{2m^2}{\pi^2}T^2\sum_{n=1}^{n=\infty}\frac{(-1)^{n+1}}{n^2}\cosh\left(n\frac{\mu}{T}\right)\left(3K_2\left(n\frac{m}{T}\right) + n\frac{m}{T}K_1\left(n\frac{m}{T}\right)\right) \tag{1.36}$$

Using recursion relations for the modified Bessel functions [22, (10.29.1)], we see that this is equivalent to the expression used in other BBN codes [7].

$$3K_2(z) + zK_1(z) = 3\frac{z}{4}[K_3(z) - K_1(z)] + zK_1(z) = \frac{z}{4}[3K_3(z) + K_1(z)] \tag{1.37}$$

$$\rho_e(T) = \frac{m^3}{2\pi^2} T \sum_{n=1}^{n=\infty} \frac{(-1)^{n+1}}{n} \cosh\left(n\frac{\mu}{T}\right)\left(3K_3\left(n\frac{m}{T}\right) + K_1\left(n\frac{m}{T}\right)\right) \tag{1.38}$$

As mentioned many older BBN codes track the parameter $\phi_e = \frac{\mu}{T}$, but this is unnecessary, as the electron density after e^- e^+ annihilation is 3 orders of magnitude lower than the already negligible contribution of the baryons. So for the remaining calculation we set $\mu = 0$.

Finding the temperature derivative of the electron energy density, can also be achieved using the recursion relations for Bessel functions [22, (10.29.2)].

$$\frac{d}{dz}\frac{1}{z}[3K_3(z) + K_1(z)] = -3[z^{-2}K_3(z) + z^{-1}K_2(z) + 3z^{-2}K_3(z)] - z^{-1}K_2 \tag{1.39}$$

$$= -12z^{-2}K_3(z) - 4z^{-1}K_2(z) \tag{1.40}$$

$$= -\frac{1}{z}[2K_4(z) - 2K_2(z) + 4K_2(z)] \tag{1.41}$$

$$= -\frac{2}{z}[K_4(z) + K_2(z)] \tag{1.42}$$

With this it is easy to determine the temperature derivative.

$$\frac{d\rho_e(T)}{dz} = -\frac{m^3}{\pi^2} T \sum_{n=1}^{n=\infty} \frac{(-1)^{n+1}}{n}\left(K_4\left(n\frac{m}{T}\right) + K_2\left(n\frac{m}{T}\right)\right) \tag{1.43}$$

$$\frac{d\rho_e(T)}{dT} = \frac{m^4}{\pi^2}\frac{1}{T} \sum_{n=1}^{n=\infty} (-1)^{n+1}\left(K_4\left(n\frac{m}{T}\right) + K_2\left(n\frac{m}{T}\right)\right) \tag{1.44}$$

1.2.4 Baryons

The temperatures at which BBN takes place are too low for Baryon pair production. Therefore, the number density of baryons can be solely determined by the scale factor and some known density.

$$n_b(a) = \frac{a_0^3}{a^3} n_b(a_0) \tag{1.45}$$

To determine baryon density $n_b(a_0)$, we use the baryon photon/ratio η.

$$n_b = n_\gamma(T)\eta \quad , \quad n_\gamma(T) = \frac{T^3}{\pi^2}\Gamma(3)\zeta(3) \tag{1.46}$$

From the CMB we can measure the value of η, during recombination, but unlike baryons the number of photons does not remain unchanged from the start of BBN until recombination. The only significant source of photons is the annihilation of the electron-positron pairs. We can account for this using conservation of entropy. For a given species we define the entropy density [8, (3.91)].

$$s = \frac{\rho + P}{T} \tag{1.47}$$

Setting $a = 1$ at the start of our BBN calculations, we get a relation between the total entropy before and after annihilation.

$$s_\gamma(T_{CMB})a_{CMB}^3 = s_e(T_i) + s_\gamma(T_i) \tag{1.48}$$

The photon number density is directly proportional to entropy density, both scaling with T^3. This allows us to restate (1.48) only in terms of the initial entropy density.

$$n_\gamma(T_{CMB})a_{CMB}^3 = \frac{n_\gamma(T_i)}{s_\gamma(T_i)}\left(s_e(T_i) + s_\gamma(T_i)\right) \tag{1.49}$$

From this we get the baryon density as a function of the initial photon and electron density and pressure.

$$n_b(a_{CMB})a_{CMB}^3 = n_\gamma(T_i)\left(\frac{s_e(T_i) + s_\gamma(T_i)}{s_\gamma(T_i)}\right)\eta \tag{1.50}$$

$$n_b(a) = \frac{1}{a^3}n_\gamma(T_i)\left(1 + \frac{\rho_e(T_i) + P_e(T_i)}{\rho_\gamma(T_i) + P_\gamma(T_i)}\right)\eta \tag{1.51}$$

With T_i being the initial temperature. Finally, to get the energy density we simply need to sum over all different nuclei.

$$\rho_b(a) = n_b(a)\sum_i Y_i m_i \tag{1.52}$$

For each isotope m_i is the mass, and Y_i is the ratio between the number of nuclei and the total number of nucleons. Y_i is often defined as $Y_i = X_i/A_i$, with X_i being the mass fraction, and A_i the atomic weight [5]. The difference in per nucleon mass of different isotopes, causes these two definitions to have a relative difference of $1e-5$, which can be safely neglected. Furthermore, since eta is only known with an accuracy of 1% [17], we can approximate that all baryons have the same mass as a lone proton reducing (1.52) to $\rho_b(a) \approx n_b(a)m_p$.

The baryon pressure can be found using the ideal gas law.

$$P_b(a) = n_b(a)T\sum_i Y_i \tag{1.53}$$

Unlike for the relativistic particles, the baryon pressure is several orders of magnitude lower than the density. Since the baryon density is already comparatively low, the pressure will be completely negligible.

1.3 Nuclear reactions

All relevant nuclear reactions involve at most 6 different nuclei. Generally we can write these reactions as

$$N_iX_i + N_jX_j + N_kX_k \leftrightharpoons N_nX_n + N_mX_m + N_lX_l, \tag{1.54}$$

where N_i is the number of nuclei X_i, that enter the reaction. The change in abundance Y_i of any nuclei is given by the sum of all reactions that create or destroy it.

$$\frac{dY_i}{dt} = \sum_{\lambda_i}\frac{N_i}{n_b}\left(\lambda_{nml\to ijk}\frac{Y_n^{N_n}Y_m^{N_m}Y_l^{N_l}}{N_n!N_m!N_l!}n_b^{(N_n+N_m+N_l)} - \lambda_{ijk\to nml}\frac{Y_i^{N_i}Y_j^{N_j}Y_l^{N_k}}{N_i!N_j!N_k!}n_b^{(N_i+N_j+N_k)}\right) \tag{1.55}$$

With λ being the reaction rate, and n_b the baryon number density. The reaction rate $\lambda(T)$ only depends on the kinetic energy of the baryons and by extension the photon temperature. $n_b(a)$ only depends on the scale factor as shown in (1.51).

From (1.55) we can quite easily determine the partial derivatives required for the construction of a Jacobian.

$$\frac{\partial}{\partial Y_j}\frac{dY_i}{dt} = -\sum_{\lambda_{ij\rightarrow}} N_i N_j \lambda_{ijk\rightarrow nml} \frac{Y_i^{N_i} Y_j^{N_j-1} Y_l^{N_k}}{N_i! N_j! N_k!} n_b^{(N_i+N_j+N_k-1)} \tag{1.56}$$

$$\frac{\partial}{\partial Y_n}\frac{dY_i}{dt} = \sum_{\lambda_{n\rightarrow i}} N_i N_n \lambda_{nml\rightarrow ijk} \frac{Y_n^{N_n-1} Y_m^{N_m} Y_l^{N_l}}{N_n! N_m! N_l!} n_b^{(N_n+N_m+N_l-1)} \tag{1.57}$$

1.3.1 Proton ⇋ neutron rate

At $T > 10^{10}$K any created nuclei will be instantly destroyed by high energy photons. This leaves only the conversion between neutrons and positrons, which is governed by the following reactions

$$n \leftrightarrow p + e^- + \bar{\nu}_e \tag{1.58}$$

$$n + e^+ \leftrightarrow p + \bar{\nu}_e \tag{1.59}$$

$$n + \nu_e \leftrightarrow p + e^- \tag{1.60}$$

The final reaction $p \leftrightarrow n + e^+ + \nu_e$ is not possible, as it would violate energy conservation, which is obvious if one considers the reaction from rest frame of the proton. For most other rates, we can measure λ experimentally for the forward rate $Q > 0$, and using detailed balance to estimate the corresponding reverse rate. The conditions required for maintaining nuclear statistical equilibrium between neutrons and protons cannot be achieved experimentally, and the rate therefore must be determined theoretically. This involves evaluating several integrals, which depend on both electron and neutrino density, in addition to the temperature and scale factor. Several corrections must also be made to account for the radiative, zero-temperature, corrections, finite nucleon mass corrections, finite temperature radiative corrections, weak-magnetism, and QED plasma effects[15]. The final result mainly depends on temperature and experimentally determined mean neutron lifetime, τ_n. Since it isn't affected by the later reactions, it is sensible to just fit the result as a function of temperature and mean lifetime. In this thesis I will use the result given in appendix C of [11], which is parametrized,

$$\lambda_{n\rightarrow p} = \frac{1}{\tau_n} e^{-q_{np}/z} \sum_{i=0}^{13} a_i z^{-i} \quad , \quad 0.01 \leq T/\text{MeV} \leq 10 \tag{1.61}$$

$$\lambda_{p\rightarrow n} = \begin{cases} \frac{1}{\tau_n} e^{-q_{pn}\cdot z} \sum_{i=0}^{10} b_i z^{-i} & , \quad 0.1 \leq T/\text{MeV} \leq 10 \\ 0 & , \quad 0.01 \leq T/\text{MeV} \leq 0.1 \end{cases} \tag{1.62}$$

With the fitted parameters being the constants a_i and b_i as well as q_{np} and q_{pn}.

1.4 Initial conditions

1.4.1 Initial temperature

When performing BBN calculations, it is most sensible to choose an initial temperature, and from it, determine all other initial conditions. The chosen temperature should be sufficiently high, so that all particles are in thermal equilibrium. Most BBN codes use 2.7e10 K as the initial temperature. Higher temperatures could be used, but this is unnecessary and will often lead to numerical instabilities, which I will touch upon in Chapter 2.

1.4.2 Initial time

Though none of the equations describing BBN, have any explicit time dependence, it is still nice to know the age of the universe when it takes place. This can be achieved by integrating equation (1.6), with $T = \infty$ at $t = 0$.

$$\int_0^{t_i} dt = -\int_\infty^{T_i} (24\pi G\rho_{tot})^{-1/2} \frac{\frac{d\rho_{set}(T)}{dT}}{\rho_{set}(T) + P_{set}(T)} dT \tag{1.63}$$

For high temperatures we can assume that the electrons are completely relativistic. Based on the result for neutrinos (1.22), we know that the energy of a massless fermion differs from that of a boson by a factor of 7/8. Accounting for the g factors, we get $\rho_e = 7/4\rho_\gamma$. At temperatures above 2 MeV the relativistic approximation deviates by less than 1%, see figure 1.1.

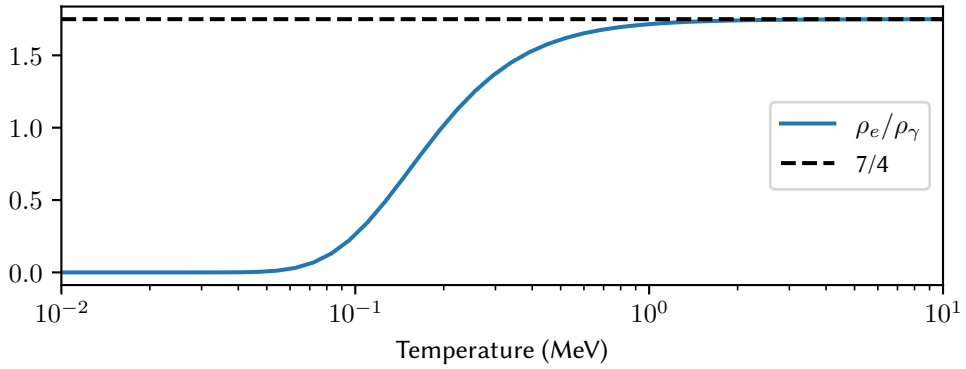

FIGURE 1.1: Exact ratio of the electron-positron energy to the photon energy.

At these temperatures we can safely ignore the baryon contribution, which combined with (1.17), allows us to calculate the non-decoupled terms.

$$\frac{\frac{d\rho_{set}(T)}{dT}}{\rho_{set}(T) + P_{set}(T)} = \frac{3}{4}\frac{1}{\rho_{set}(T)}\frac{d\rho_{set}(T)}{dT} = 3T^{-1} \tag{1.64}$$

For the total energy we simply add the contributions of all components, excluding baryons,

$$\rho_{tot} = \rho_\gamma + (2+3)\frac{7}{8}\rho_\gamma = \frac{43}{8}\rho_\gamma \tag{1.65}$$

Inserting into (1.63), we get the initial time,

$$t_i = 3(24\pi G\frac{43}{8}\frac{\pi^2}{15})^{-1/2}\int_{\infty}^{T_i} T^{-3}dT \tag{1.66}$$

$$t_i = \frac{3}{2}(\frac{43}{5}G\pi^3)^{-1/2}T_i^{-2} \tag{1.67}$$

This relation is valid at all times before decoupling, and remains approximately true at later times, as shown on figure 1.2.

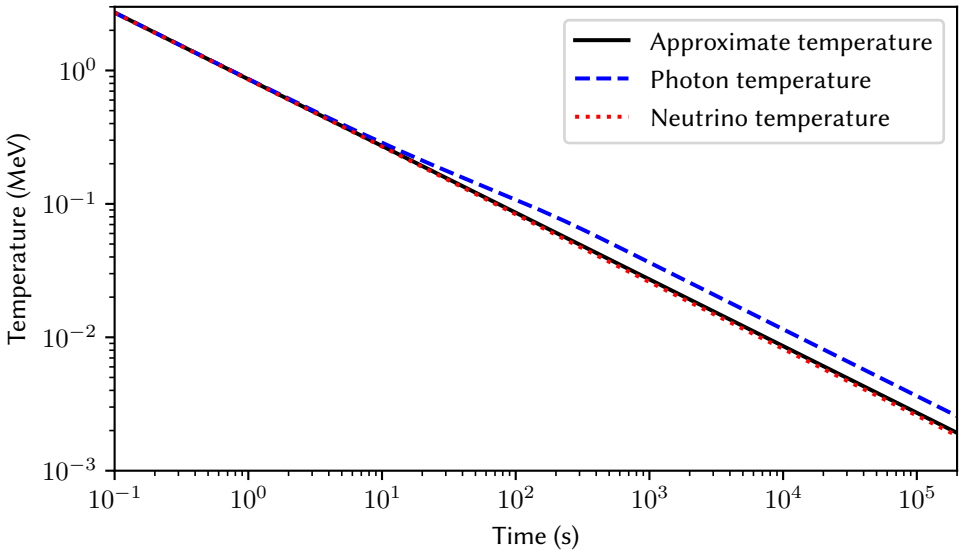

FIGURE 1.2: The temperature of photons and neutrinos during the time period of BBN, as well as the approximate temperature given by 1.67.

To get a sense of scale for this result we can rewrite it in units of 10^9K and seconds.

$$T_9 = (43\frac{4}{3}\pi\frac{a}{c^2}G)^{-1/4}t^{-1/2} = 9.97t^{-1/2}, \tag{1.68}$$

with a being the radiation constant, related to the Stefan–Boltzmann constant by $a = \frac{4}{c}\sigma$. Using this we can justify the omission of particles heavier than electrons. The lightest of these are the muon and pion, which both have masses above 100 MeV. Significant pair creation will occur at $T_9 \geq 10^3$, corresponding to $t \approx 10^4$. As such they will have no significant impact on the initial time.

We note that (1.68) differs significantly from the expression derived by Wagoner[4],

$$T_9 = (12\pi\frac{a}{c^2}G)^{1/4}t^{-1/2} = 10.4t^{-1/2}, \tag{1.69}$$

The analytical expression is wrong, but the numerical result is correct. A simple error which probably was the result of a small mistake when transcribing the notes used for the paper. Unfortunately, this expression has been reproduced in several

later BBN codes such as NUC123[7] and AlterBBN[16]. Though Kawano reproduced the equation in the documentation, in the actual NUC123 code he used the numerical result and as such the code itself had no errors. In AlterBBN they used natural units, and so couldn't use the numerical value, leading to the error affected the code. Additionally, they also confused the Stefan–Boltzmann and radiation constants leading to an additional error. Examining the code, one can see that their value is wrong by 14 orders of magnitude. Since it doesn't impact final abundances, this error was only very recently discovered. The first correction being released in 2021 by Sharpe [19],

$$T_9 = (48\pi \frac{a_r}{c^2} G)^{-1/4} t^{-1/2} = 10.4 t^{-1/2}, \tag{1.70}$$

However this still differs from (1.68). This due to the fact that the original derivation was performed by Wagoner in 1967, a decade before the discovery of the Tau and corresponding neutrino. And though later projects correctly added the additional neutrino flavor when calculating the neutrino energy, the impact it has on the initial time had been overlooked before this thesis.

Chapter 2

BBN code

2.1 A brief history of BBN codes

The concept of Big Bang nucleosynthesis is almost as old as the Big Bang theory itself, with the with it first being proposed in the paper by Alpher, Bethe, and Gamow [2]. This early model used neutron capture and subsequent beta decay as the mechanism for BBN, though its greatest problem was the inability to explain the unusually high abundance of oxygen and carbon in the present universe. And so, it was in large part supplanted by the new theory of stellar nucleosynthesis, as the main explanation for the origin of elements.

During the next decades it became clear that stars could not be the only explanation for the present element abundances, and with the discovery of the CMB in 1965, new attention was brought to the early universe. Only a year later Peebles showed how simple BBN physics could be used to explain the high helium abundance, unaccounted for by stellar nucleosynthesis [3].

In the following years Wagoner created and refined the first proper BBN code, described in a series of defining papers[4][5][6]. With the legacy of this code still heavily influencing the way BBN calculations are performed today.

By the late 80s the Wagoner code was severely outdated. With multiple inefficiencies due to among other things, the fact that it was originally designed to run on punch cards. This inspired Lawrence Kawano to create the now ubiquitous NUC123, colloquially know as the Kawano code[7]. Which set the gold Standard for all future BBN codes.

2.1.1 Modern codes

In current day and age, there exists multiple publicly available BBN codes, and a countless number of private codes. The most well know of these are PArthENoPE, AlterBBN, and PRIMAT.

PArthENoPE[20] is a spiritual successor to NUC123, and like the works of Wagoner and Kawano PArthENoPE uses FORTRAN. It retains the same structure, and can generally be seen as a continually updated version of these earlier works, with features such as updated reaction rates and a user-friendly GUI.

PRIMAT[15] is a Mathematica code and unlike PArthENoPE and AlterBBN, it isn't directly based on the older BBN codes. The main focus of PRIMAT is improving the precision of BBN codes specifically the He4 abundance, which is mainly determined by the $p \leftrightharpoons n$ rates.

AlterBBN is written in c and based on Kawano's NUC123. It maintains the same basic structure and integration method, though it uses natural units for everything but the reaction network. However, they define energy in GeV rather than MeV. What separates AlterBBN for other codes is that as the name implies, it allows the use of alternate cosmological models and parameters. Therefore, this code is especially well suited for testing the effects these alterations have on final abundances.

2.2 Integrating the system of equations

The objective of any BBN code is to solve the system of differential equations described in chapter 1, which presents some numerical difficulties.

Most nuclear reactions have a linear or quadratic dependence on density, as well as an often exponential dependence on temperature. At high temperatures this is balanced by the corresponding reverse rate being equally high. The forward and reverse rates will only cancel at the precise abundance required by nuclear statistical equilibrium (NSE). Any slight deviation from NSE δY, will cause one rate to be slightly larger, which due to its magnitude will cause a huge increase in the derivative Y'.

Most numerical methods for solving differential equations are explicit, and in their simplest form calculate the next step by adding $\Delta Y = \Delta t \cdot Y'$. If $\Delta Y > 2\delta Y$, the system will become unstable as each step will increase the absolute value of both. To avoid this instability an explicit method will have to use a minuscule step size Δt, which in practice makes the problem unsolvable.

This and similar problems are called stiff, since they are very inflexible when faced with slight deviations from the "true" solution.

Integration methods

Wagoner and the later codes based on this work handle the stiffness by first linearizing the system, which allows integration in an implicit form:

$$\tilde{Y}_{n+1} = (1 + C\Delta t)\tilde{Y}_n \approx (1 - C\Delta t)^{-1}\tilde{Y}_n. \tag{2.1}$$

This is then followed by a traditional second order Runge-Kutta integration, with AlterBBN having options for more advanced Runge-Kutta methods.

PRIMAT on the other hand uses a first order BDF scheme for $T > 1.25\text{e}9$ K, switching to second order at lower temperatures for faster computation.

I have chosen to use an implicit Runge-Kutta method of the Radau IIA family of order 5, as implemented in SciPy[18]. This method is perfectly suited to handle stiff problems such as the reaction network, and based on testing it is the most stable method among those available in SciPy.

2.2.1 Simplifications of the problem

Following the example of Wagoner, most BBN codes solve the background variables and abundances concurrently. This is necessary as they account for the change in baryon energy density and electron chemical potential caused by nucleosynthesis. Accounting for the baryon energy only results in a relative abundance change lower than 10^{-5} for the heavier nuclei, and even less for lighter ones. Accounting for baryons at all is questionable, and tracking the abundance of non-thermal electrons and energy changes caused by nucleosynthesis is completely unnecessary. Accordingly, the background variables can be treated as independent of the abundances.

This is beneficial, as unlike the abundances the equations governing temperature and scale factor are not stiff in the slightest. This allows faster integration, with fewer evaluations of computationally demanding terms such as the sum in electron energy density (1.36). Barring e^- e^+ annihilation, T and a follow the simple power laws $T^{-2} \propto t$ and $a^2 \propto t$, as seen on figure 1.2. This allows the use of simple linear interpolation in log space, which will have negligible impact on runtime compared to the evaluation of reaction rates.

Compared to the background parameters, evaluating reaction rates is quite simple, with the most time-consuming part being the sheer number of rates, which can be mitigated somewhat with parallelization. Here the main problem is the aforementioned stiffness, but this is also aided by precomputing the background variables, as this demonstrably improves stability.

2.3 Creating the reaction network

To create the reaction network I use pynucastro[21], which is an open source python interface designed for nuclear astrophysics. The reaction rates themselves are provided by the REACLIB database[12]. These rates are based on fits of experimental results using the following parametrization

$$\lambda = \exp\left(a_0 + \sum_{i=1}^{5} a_i T_9^{\frac{2i-5}{3}} + a_6 \log T_9 \right). \tag{2.2}$$

T9 is the temperature in 1e9 K, and the molar density must be provided in cgs units of mol/cm^3. Converting from natural units to cgs is a simple matter of multiplying by $\frac{MeV}{\hbar c}^3 \frac{1}{N_0} = 2.161\text{e}8\,\text{cm}^{-3}$, with N_0 being the Avogadro number. For some reactions such as those with powerful resonances, a rate can be comprised of multiple terms of the form given in (2.2), to allow for more accurate fit of the data.

To create the network, pynucastro must first be provided with the list of included nuclei. It has a built-in method for collecting all reactions between these nuclei which creates a library object containing the rates and their relations. This can then be used to generate a python file which takes density, temperature and abundances as inputs and returns the rhs and Jacobian. This file supports just in time compilation using the JIT module from Numba, which takes between a few seconds to a few minutes depending on the size of the network. To avoid having to compile the networks every time I modify the code, I added a method that compiles the network ahead of time using the Numba CC module.

At high temperatures heavy nuclei have extremely low abundances while greatly increase the stiffness of the system. To increase both stability and performance, it is prudent to extend the network gradually, which can be accomplished by using 3 different reaction networks.

At very high temperatures, deuterium is readily destroyed by high energy photons inhibiting the production of any subsequent nuclei. Here the simplest possible reaction network is employed, comprised of only the proton, neutron, their forward and reverse rate.

When temperatures are low enough to allow deuterium production then network is extended to include all nuclei with $A \leq 7$, see figure 2.1. This accounts for the nuclei involved in ^{4}He production and their immediate fusion products, which are also the only nuclei with observable final abundances.

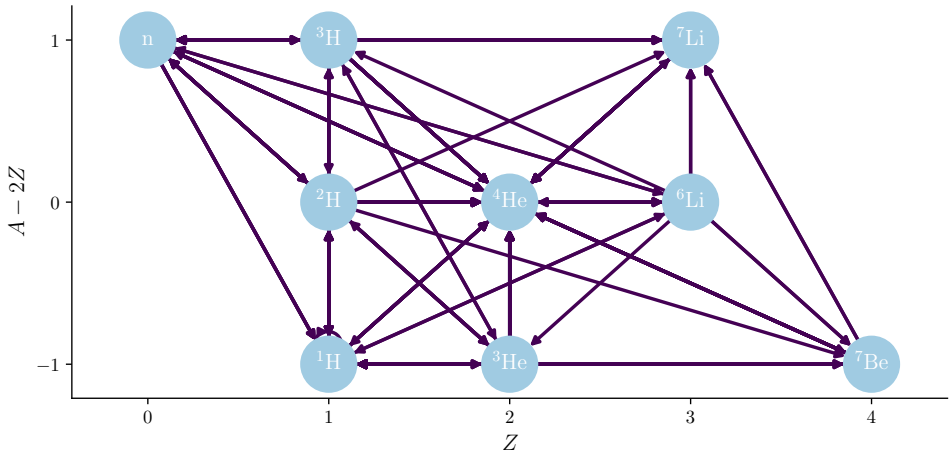

FIGURE 2.1: Reduced reaction network for calculating light element abundances at high temperatures, with arrows representing forward reaction rates.

When significant amounts of ^{4}He and heavier nuclei have formed, we switch to the full network which includes every nucleus that could possibly affect BBN, see figure 2.2. Due to the extreme temperature dependence of reactions such as triple alpha, this network is very stiff at high temperatures.

2.4 Running the code

- We use pynucastro to generate the reaction networks. This is by far the most time-consuming step, but unless we need to modify a reaction rate, we only need to do it once.
- The time evolution of background parameters is calculated and stored. To speed up subsequent calls to the background parameters, JIT is use for the interpolation function.
- Initial conditions are set based on the background parameters, with the proton and neutron abundance being determined from NSE.

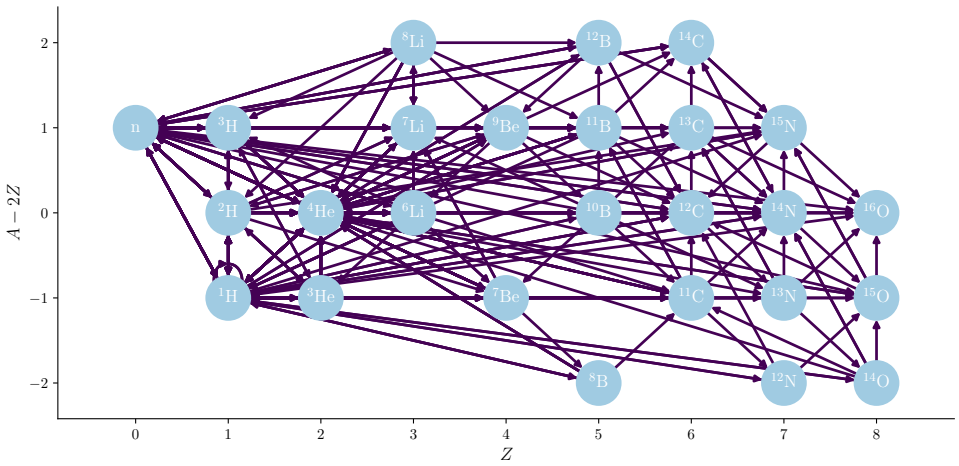

FIGURE 2.2: Full reaction network for more precise determination of heavy element abundances at intermediate to low temperatures, with arrows representing forward reaction rates.

- The first reaction network is integrated, from a specified initial time until the switch to the second network.
- Before beginning integration the second network, the initial abundance of the added nuclei is determined by requiring that the resulting right-hand-side (RHS) is 0. This minimizes the transients created as the new nuclei rapidly readjust due to the stiffness of the system.
- The second reaction network is integrated using these initial conditions, after which the same procedure is used for the third network.
- Barring the addition of additional reaction networks, we get the final abundances, as well as their evolution over time.

Chapter 3

Output

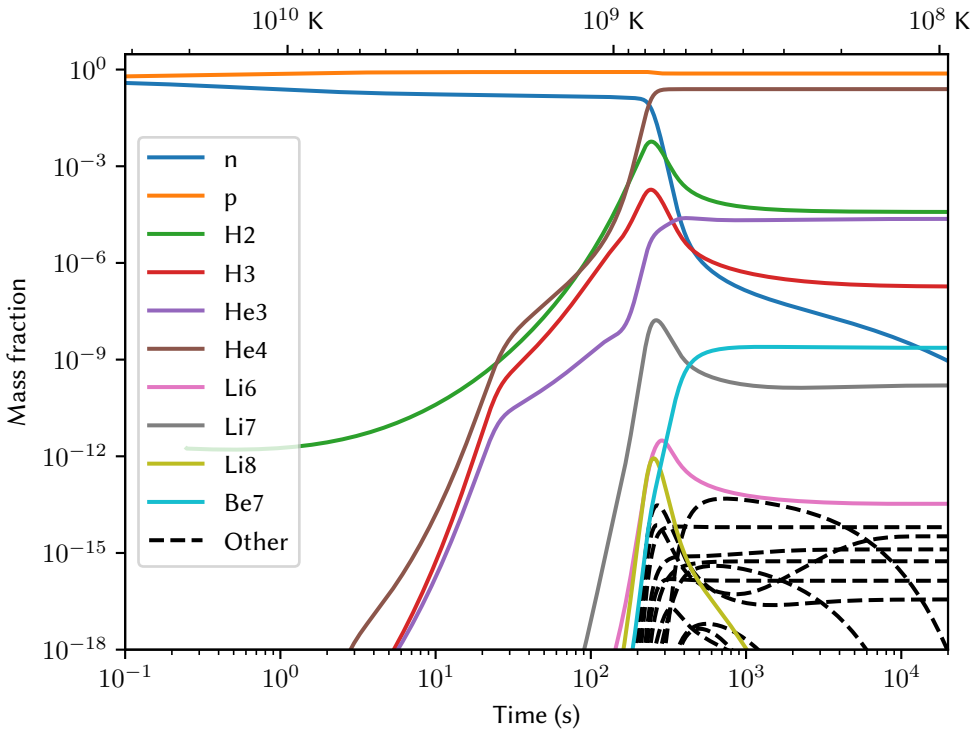

Figure 3.1: Time evolution of light nuclei abundance during BNN, with mass fraction technically being the close approximation $X_i = Y_i A_i$.

Running the code creates a complete overview of abundance evolution as shown on figure 3.1. As expected neutrons protons and deuterium remain in equilibrium for the first few seconds. As the temperature decreases, deuterium abundances slowly increase quickly followed by tritium and both helium isotopes. This continues until around 230 seconds, at which point the rate of ^{4}He creation is finally great enough to have a significant impact on neutron abundance, which until then had remained

almost unchanged since the $p \leftrightarrow n$ rates fell out of equilibrium. This leads to a rapid drop in neutron abundance creating a bottleneck on the production of deuterium and tritium. Without neutron capture to create more, the existing deuterium and tritium is converted to ^{4}He via $^3\mathrm{H} + {}^2\mathrm{H} \rightarrow {}^4\mathrm{He} + n$. Without these light nuclei lithium abundances also drop, as reactions such as $^4\mathrm{He} + {}^3\mathrm{H} \rightarrow {}^7\mathrm{Li}$ become outmatched by the proton captures $^7\mathrm{Li} + \mathrm{p} \rightarrow 2\,{}^4\mathrm{He}$ and $^6\mathrm{Li} + \mathrm{p} \rightarrow {}^7\mathrm{Be}$. Conversely, Beryllium 7 is primarily destroyed via neutron capture $^7\mathrm{Be} + \mathrm{n} \rightarrow {}^7\mathrm{Li} + \mathrm{p}$, and therefore sees a rapid increase in abundance immediately after the drop in neutrons.

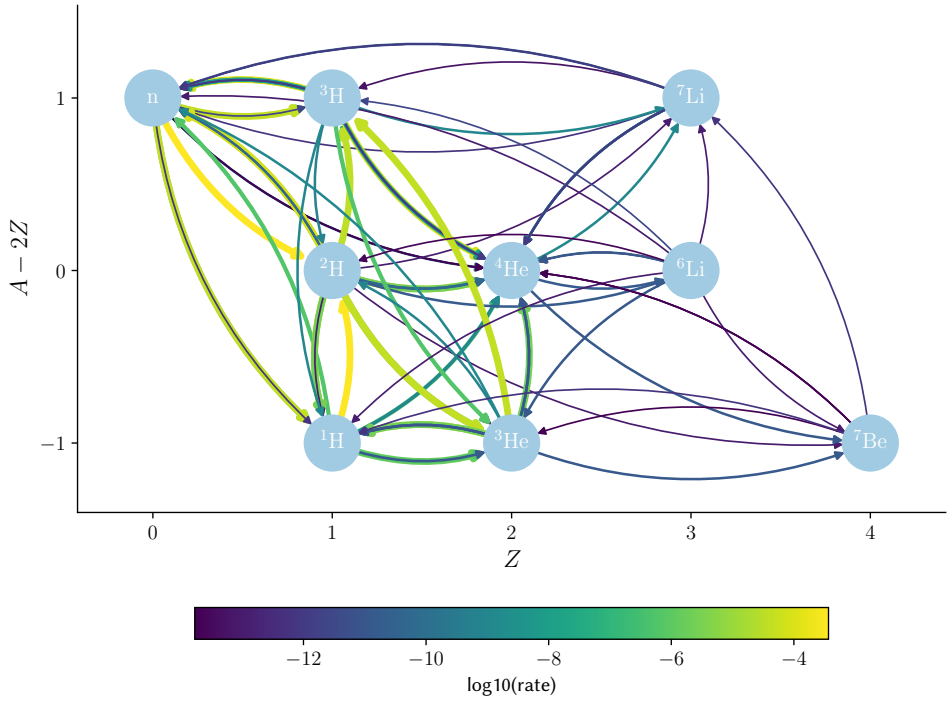

FIGURE 3.2: Reaction rates 5 minutes after Big Bang at 7.6e8 K. Only including rates within 10 orders of magnitude of strongest. Each rate is represented by arrows from each reactant to each product.

The relations of these reactions are illustrated in figure 3.2. This snapshot is taken immediately after the aforementioned drop in neutron abundance with $Y_n = 0.2\%$. Despite this $n + p \rightarrow d$ is still the strongest reaction rate, followed by rates creating ^{3}He and ^{3}H, simply due to the high abundance of these light nuclei. Though no particular reaction is exceptionally strong, a disproportionate amount of reactions produce rather than consume ^{4}He. This should come as no surprise as ^{4}He is the most tightly bound of all these nuclei. The only rates consuming helium are those producing heavier elements, $^4\mathrm{He} + {}^3\mathrm{H} \rightarrow {}^7\mathrm{Li}$, $^4\mathrm{He} + {}^3\mathrm{He} \rightarrow {}^7\mathrm{Be}$, and $^4\mathrm{He} + {}^2\mathrm{H} \rightarrow {}^6\mathrm{Li}$. Yet these barely affect total helium abundance, and to an extent help create more ^{4}He through subsequent reactions such as $^7\mathrm{Li} + {}^2\mathrm{H} \rightarrow 2\,{}^4\mathrm{He} + \mathrm{n}$.

The most striking effect of the high ^{4}He binding energy is the lack of stable nuclei with $A = 8$, due 2 alpha particles being energetically favorable. Many nearby nuclei are also unstable creating a gap in the full reaction network, apparent on

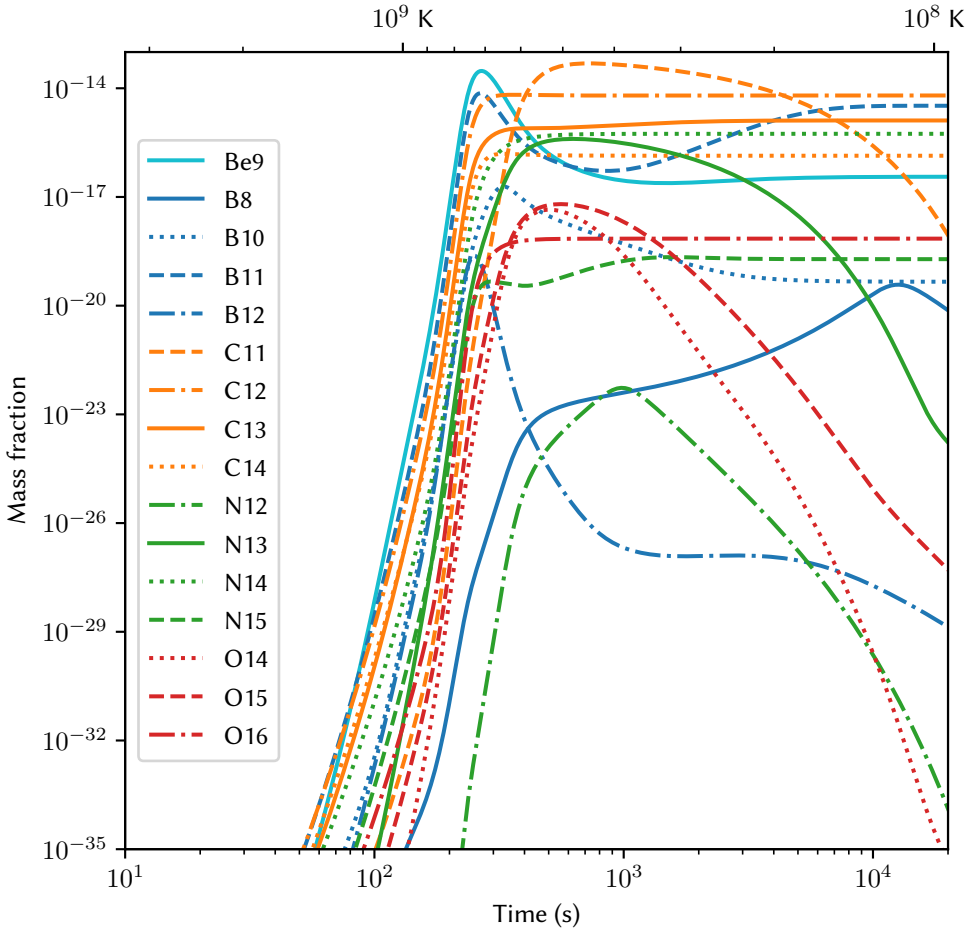

FIGURE 3.3: Time evolution of heavy nuclei abundance during BNN, with mass fraction technically being the close approximation $X_i = Y_i A_i$.

2.2. The next nucleus with greater binding energy per nucleon is ^{12}C, which after BBN is also the most abundant of the heavy nuclei, as seen on figure 3.3. Bridging the gap between ^{4}He and ^{12}C is usually accomplished via the triple-alpha process $3^4\text{He} \rightarrow {}^{12}\text{C}$, which occurs in stars at temperatures above 10^8K. The temperature during BBN is even higher than this, but compared to stellar interiors the density is much lower. At the previously mentioned 5 minute mark, the baryon density of the universe is only 10 grams per cubic meter, which is more than ten orders of magnitude lower than that of a helium burning stellar core. This completely stops the triple-alpha process, leaving the inefficient process of alpha capture on ^{7}Li and later ^{7}Be as the only options for creating heavier nuclei. This firstly creates ^{11}B, which is through proton capture is responsible for the majority of ^{12}C production. Unfortunately the resulting exited state $^{12}\text{C}^*$ predominately decays into three alpha particles, with the branching ratio of internal translation into the ground state being only $1.5e-4$. The same is true for neutron capture on ^{11}C, though it also decays via proton emission $^{12}\text{C}^* \rightarrow {}^{11}\text{B} + \text{p}$ and of course freely decays $^{11}\text{C} \rightarrow {}^{11}\text{B}$. From figure 3.3 we also see an initial bump in ^{9}Be abundance caused by the uniquely high

cross-section of the reaction $^7\mathrm{Li} + {}^3\mathrm{H} \rightarrow {}^9\mathrm{Be} + n$, but as tritium abundance drops most ^{9}Be is destroyed by photofission $\gamma + {}^9\mathrm{Be} \rightarrow 2{}^4\mathrm{He} + n$.

3.1 Precision

Throughout the code there are several places where numerical accuracy must be balanced by the need for swift computation. As a baseline I aim for a relative precision on final abundances of 10^{-5} due to numerical uncertainty. This is much lower than the error introduced by the experimental determination of reaction rates, as well as that of astronomical observations of primordial abundances.

3.1.1 Tolerances

For the integration itself I use the solve_ivp method from scipy.integrate[18]. Here ensuring numerical accuracy is a simple matter of specifying the desired relative and absolute tolerances as optional parameters, which I have set as rtol=1e-6 and atol=1e-80. The absolute tolerance might seem exorbitantly low, but this helps improve stability since some heavy nuclei can cause detrimental transients if not tracked accurately at even minute abundances. However, for the tests this section I use rtol=1e-8, to ensure any inaccuracy is caused be whatever parameter is being tested.

3.1.2 Electron energy

Most calculations for the background have nice analytical expressions that can be computed with arbitrary precision. The electron energy density is the main exception, as it is given by an infinite sum (1.36) of which a finite number of terms must be calculated. Electrons annihilate very early, so any error in the energy density will only affect the $p \leftrightharpoons n$ rate. This will lead to a small change in neutron abundance, which results in a similar (within one order of magnitude) relative change in the abundance of all subsequent nuclei. Testing shows that small changes to the energy density, cause a change in neutron abundance of roughly the same relative magnitude if not slightly lower. So to achieve the requested accuracy in abundance, I will also aim for a 10^{-5} relative error in total energy density.

Figure 3.4 shows the deviation from the reference energy at select temperatures before and during e^- e^+ annihilation. For low temperatures the sum converges quickly, which should come as no surprise as the series in (1.31), converges more rapidly as $e^{-(E\pm\mu)/T}$ approaches 0. At high temperatures the sum converges at a much slower rate, but it still achieves sufficient accuracy with only 20 terms, which is the number I will use moving forward.

3.1.3 Interpolation

For the interpolation on background variables an appropriate number of points must be selected. These points are spaced uniformly in log(t). Tests show that 10^4 points is sufficient to achieve the required accuracy in final abundances. However, a low number of points cause the small discontinuities in the derivatives of temperature

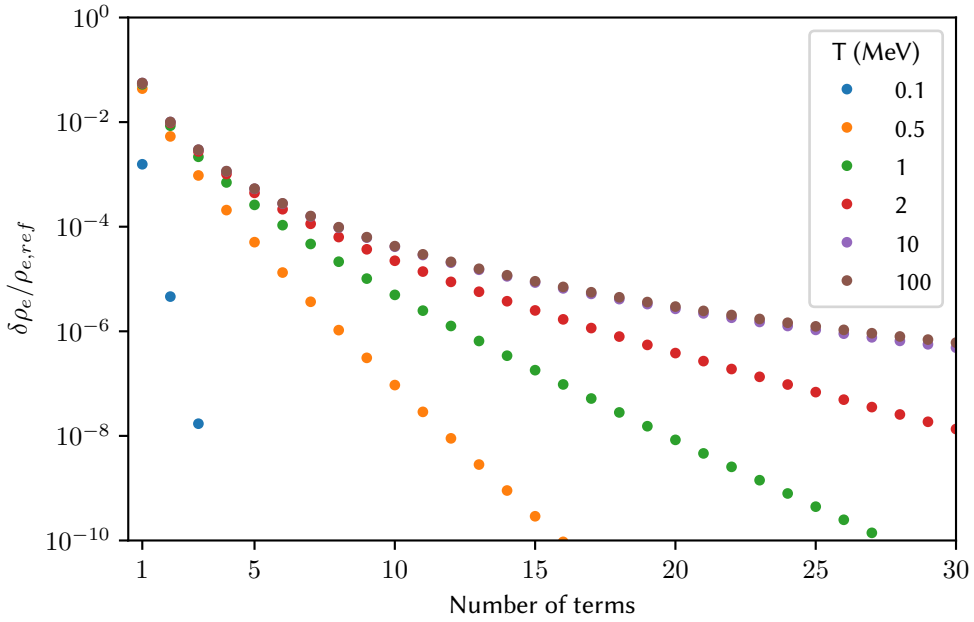

FIGURE 3.4: Normalized absolute deviation of electron energy density from the reference energy as a function of included terms in (1.36). The reference energy density has been determined by computing the first 10000 terms.

and scale factor. Due to the stiffness of the system this leads to instabilities, which have a major impact on the runtime. At the required resolution of 10^4 the integration routine has to make twice as many call to the RHS, compared to smoother integration. At 2×10^5 points the interpolations is smooth enough as to not cause issues for integration.

3.1.4 Network timings

As mentioned in section 2.3, we cannot calculate the abundance of all nuclei from the beginning, and have to add them gradually as the y become relevant. To find this point we can plot the deviation in final abundance as a function of the time at which we switch between networks.

Full network

We start by looking at the full network shown on figure 3.5, which has three distinct points. As long as the heavy nuclei are added before 2 minutes corresponding to $T > 10^9$K they have time to reach the same abundance as they would if they were added earlier. Adding them later will delay the initial production, which will slowly lower the resulting final abundance. They will however still reach approximately the same final abundance until the late stages of BBN at around 7 minutes. Here the temperature will be to low for their formation, resulting in an increase in Lithium and Beryllium, as these are no longer consumed to produce heavy nuclei. The reaction involving ^{11}C however come into effect much later than most other reactions and remain relevant even an hour after BBN. If ^{11}C is added after this point, it will never

achieve a significant final abundance, leading to a drop in its indirect daughter nuclei ^{9}Be and ^{6}Li.

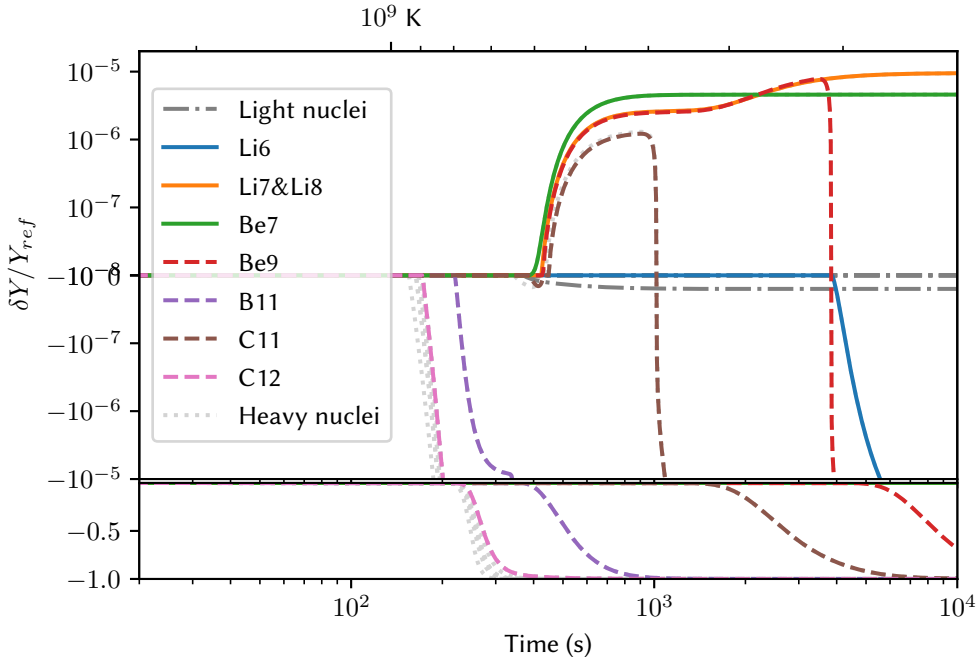

FIGURE 3.5: Relative deviation on final abundances based on the time from which heavy nuclei are included in the reaction network. To display both positive and negative changes, relative deviations $< 10^{-8}$ are excluded. The bottom shows negative deviation on a linear scale.

The result of this test shows that for standard BBN heavy nuclei don't actually need to be included at all, if one is only interested in abundances of light nuclei. For completeness, I will choose to include these nuclei anyway starting at $T > 10^9$K.

Light network

From figure 3.6 we see that delaying the calculation of nuclear abundances, initially cause an increase abundance of protons and the proton dominated nuclei ^{3}He and ^{8}B, with all other abundances dropping. This is due to early nuclear reactions trapping neutrons in the cores light nuclei such as ^{4}He and ^{2}H, preventing their free decay into protons. However, since the vast majority of neutrons are still unbound, this effect will be insignificant until large light nuclei abundances are attained. Therefore, we actually don't need to calculate early abundances to get precise estimates of the final abundance.

Not having to solve the reaction network at high temperatures makes the system much less stiff, potentially allowing future BBN codes to use less complex integrations routines than those used by this and older codes. Unfortunately starting abundance calculations presents a major issue due to the initial conditions. When starting light abundance calculation at early times $t < 10$s, we can determine the initial abundances by setting the RHS to 0 as described in section 2.4. But at later times

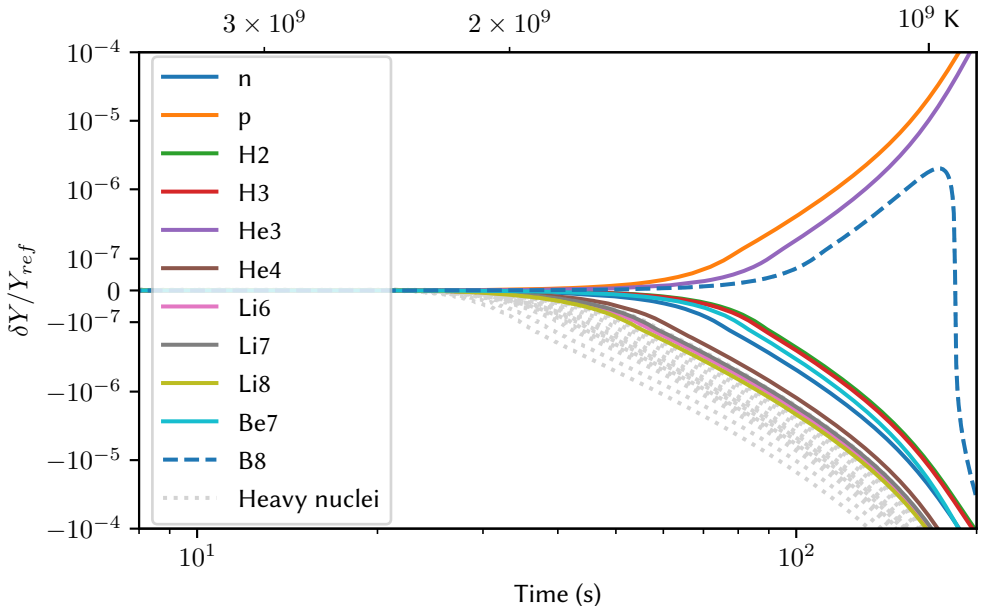

FIGURE 3.6: Relative deviation on final abundances based on the time from which light nuclei are added to the reaction network. Plot is linear in the region $\pm 10^{-7}$ and logarithmic outside.

reactions destroying ^{4}He drop off, with ^{4}He abundances instead being kept in check by the lack of deuterium. As the system is no longer in exact NSE, any method for determining initial condition which assume a steady state solution will fail. Given enough time all neutrons will be converted to ^{4}He, and the estimated initial conditions reflect this by vastly overestimating ^{4}He abundances. To get around this and produce figure 3.6, I instead had to set all initial abundances to 0 when initiating the light network after 3 seconds. This workaround eliminates the problem, but creates another in the form of transients create as abundances go from 0 to their appropriate value. Since the system of equations is less stiff at these late times the transients won't break the integration. But dealing with these transients takes just as long as the time required for just tracking abundances at early times.

$p \leftrightharpoons n$ network

Unlike the heavier nuclei the at which we start calculating neutrons and protons abundances have a very abrupt and significant impact on final abundances. As long as they are still in thermal equilibrium when we begin calculations, the final abundance will be the same. Conversely, if we start after they begin to fall out of thermal equilibrium, all final abundances will be radically different. From figure 3.7 it's clear that this occurs at around 100 ms or 3e10K, and as long as we initiate $p \leftrightharpoons n$ before this we get precise results. This also justifies the use of 27e9 K as the initial temperature, which is the point used by among others Wagoner, Kawano, and AlterBBN.

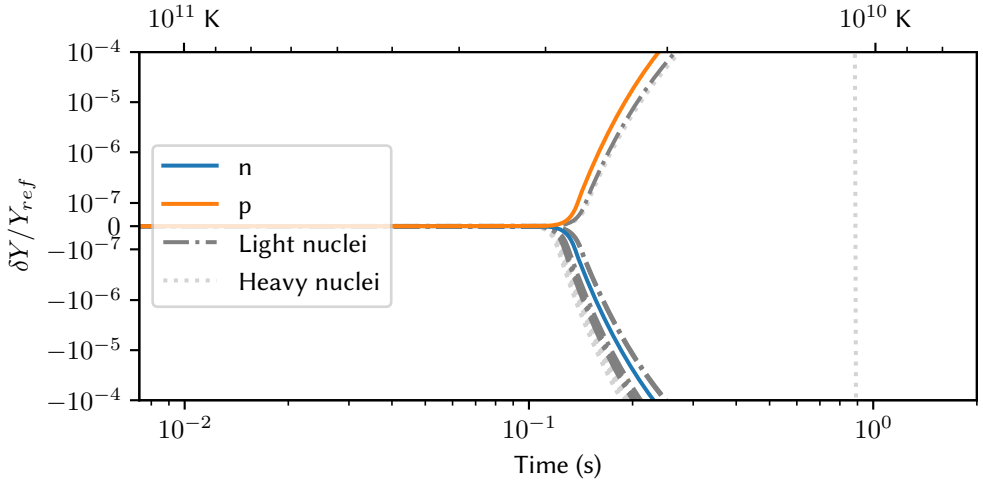

FIGURE 3.7: Relative deviation of final abundances based on the initial time of BBN calculations. Plot is linear in the region $\pm 10^{-7}$ and logarithmic outside.

3.1.5 Neutrino decoupling

The main source of inaccuracy in this code is the assumption of complete neutrino decoupling. This assumption is reasonable as the only net transfer of energy between different particles is annihilation of electrons and positrons, which begins at around 1 MeV as shown on figure 1.1. This is long after the neutrinos have decoupled, and therefore the energy is transferred to the photons, which are heated relative to the neutrinos by the well known factor $\sqrt[3]{11/4}$. There is however a small transfer of energy before the neutrinos completely decouple from the other particles. The result of this is a small increase in neutrino temperature relative to photon temperature of less than 1% [9]. As both neutrinos and photons are ultrarelativistic, this change is inconsequential to the time evolution of the early universe, and should intuitively not have a significant impact on final abundances. This is however not the case, as is apparent from figure 3.8. The reason for this is that the higher photon temperature caused by instantaneous decoupling, effectively delays the onset of nucleosynthesis, since the baryons take longer to cool sufficiently. This has two main effects, the first being slightly lower baryon density at any given temperature, and the second that the universe will remain in any given temperature range for longer. Additionally, neutrino decoupling also affects the $p \leftrightharpoons n$ reactions directly, as these rely on both exact temperature and non-thermal energy distribution of the neutrinos. When assuming complete neutrino decoupling, these effects lowers the abundance of ^{4}He by 0.05%, ^{3}He by 0.1%, and deuterium by 0.5%, and increase ^{7}Be by 0.5%, (PRIMAT table V[15]).

Since my implementation uses estimated $p \leftrightharpoons n$ rates which do take into account incomplete neutrino decoupling, my results are primarily affected by the delaying of nucleosynthesis, caused by the inaccurate $T_\nu/T\gamma$ ratio. To reduce the deviation in $T_\nu/T\gamma$ ratio, we can decouple the neutrinos as close as possible to the point at which they actually decouple. This still assumes an instant rather than gradual decoupling, but nonetheless improves predicted abundances. The point at which neutrinos decouple obviously coincide with the freezeout of $p \leftrightharpoons n$ reactions, and as

shown on 3.7, we can safely begin both background and network integration at 27 GK corresponding to 2.3 MeV.

	$Y_p \times 10$	^{2}H×10^5	^{3}He×10^5	^{7}Li ×10^{10}	^{6}Li ×10^{15}	^{7}Be ×10^{10}
100 MeV	2.470	2.532	1.040	4.712	7.503	4.411
2.3 MeV	2.472	2.536	1.040	4.706	7.523	4.404
Deviation	0.07%	0.15%	0.04%	-0.15%	0.25%	-0.18%

TABLE 3.1: Comparison of final abundances for instant decoupling at 2.3 and 10 MeV, with all abundances except ^{4}He (Y_p) being normalized to H abundance. ^{3}He and ^{7}Li including contribution from eventual decay of ^{3}H and ^{7}Be.

From table 3.1 we clearly see the impact of neutrino decoupling. Compared to the expected changes determined by PRIMAT[15], we see an increased impact on ^{4}He and a reduced impact on ^{7}Be and ^{3}He. This can mostly be explained by the $p \leftrightharpoons n$ reactions not being directly impacted in my implementation. The direct effect on $p \leftrightharpoons n$ increases the neutron abundance subsequently the abundance of all other nuclei, counteracting the effects on everything but ^{7}Be, as well as ^{3}He since its abundance actually increases as neutron abundance drops.

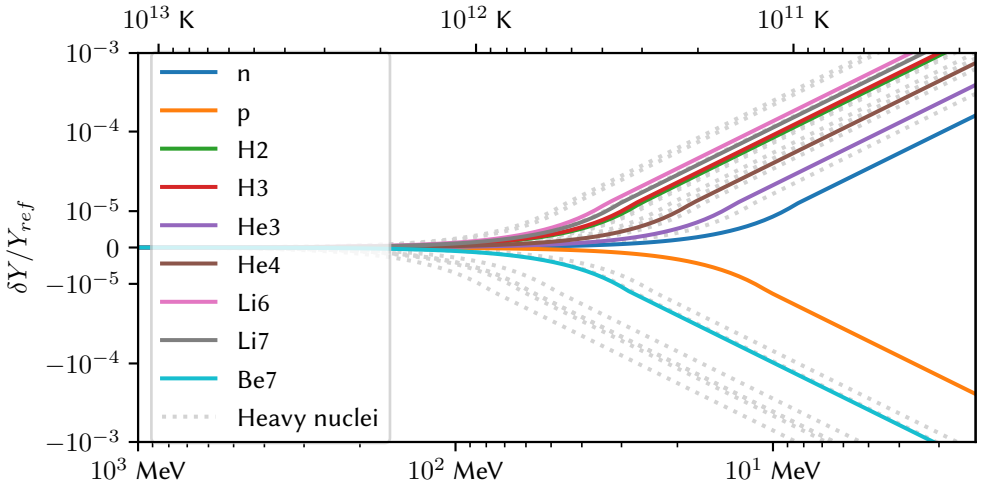

FIGURE 3.8: Relative deviation on final abundances based on the initial time for background calculations. By construction the initial time coincides with the time of neutrino decoupling.

Though the errors associated neutrino decoupling are much greater than the achieved numerical error of less than 10^{-5}, they are still acceptable, since they are completely inconsequential next to the uncertainty associated with reactions rates, as will become apparent in the following section.

3.2 Comparison with AlterBBN

To compare the results of this code to that of other contemporary BBN codes, I have chosen AlterBBN. The main reason for this is that my code is written in Python with much of the heavy computation being done directly in C. This makes it easier

	$Y_p \times 10$	^{2}H×10^5	^{3}He×10^5	^{7}Li ×10^{10}	^{6}Li ×10^{14}	^{7}Be ×10^{10}
This work	2.472	2.536	1.040	4.706	0.752	4.404
AlterBBN	2.474	2.467	1.034	5.363	1.087	5.075
+/−	0.003	0.038	0.016	0.352	1.085	0.343

TABLE 3.2: Abundances from this work and AlterBBN, with all abundances except ^{4}He (Y_p) being normalized to the H abundance. ^{3}He and ^{7}Li including contribution from eventual decay of ^{3}H and ^{7}Be. Quoted uncertainties are those determined by AlterBBN.

to interface with the C based AlterBBN than PArthENoPE or PRIMAT, which as previously mentioned are written in FORTRAN and Mathematica.

Comparing the final abundances predicted by this code and AlterBBN we see major discrepancies. Most of these are within the uncertainties calculated by AlterBBN based on the uncertainty of the reaction rates. ^{7}Be and subsequently ^{7}Li deviate by more than twice what is predicted, and the same is true for deuterium. To discover the cause of this we can do a 1 to 1 comparison of the time evolution of the universe according to this work and AlterBBN. Here we use the exact same initial conditions of $T = 27 \times 10^9$K, η = 6.1e-10 and τ_n = 880.2s, remembering to correct for the inaccurate initial time in AlterBBN as explained in section 1.4.2.

3.2.1 Background

To rule out cosmological differences, we can compare the predicted background parameters from AlterBBN and this code, displayed on figure 3.9. Unsurprisingly after the common initial temperature of 27GK, AlterBBN sees a relative increase in neutrino temperature due to incomplete neutrino decoupling, with photon temperature initially decreasing slower due to sharing temperature with the electrons. Later there is a small additional drop in photon temperature coinciding with the onset of primary nucleosynthesis. This can be explained by AlterBBN taking into account the effect of nucleosynthesis on photon temperature, due to the energy release of nucleosynthesis. However, the observed effect is unphysical and must be due to numerical errors, since the energy release is nowhere near the amount required for an impact on photon temperature of this size, and additionally it should serve to increase, rather than decrease the photon temperature. Lastly, there is a relative decrease of the AlterBBN neutrino temperature at late times. This is due to AlterBBN taking into account both baryon and dark matter energy density, which I have omitted since it clearly doesn't have a significant impact during the era of BBN.

To see the impact of these background differences we can integrate the reaction network using the background parameters from AlterBBN. At its highest precision setting AlterBBN takes 64421 discreet time steps, which based the test in section 3.1.3 is sufficient to achieve high accuracy with the existing interpolation routine. AlterBBN does however not directly track the scale factor, so we must instead track the baryon density using the neutrino temperature. Since the tabulated $p \leftrightharpoons n$ rates used in this network only depend on temperature, we don't need to know the exact value of n_b before the other reactions become relevant at around 100 seconds, (figure 3.6). At this time neutrinos have actually decoupled completely, and therefore

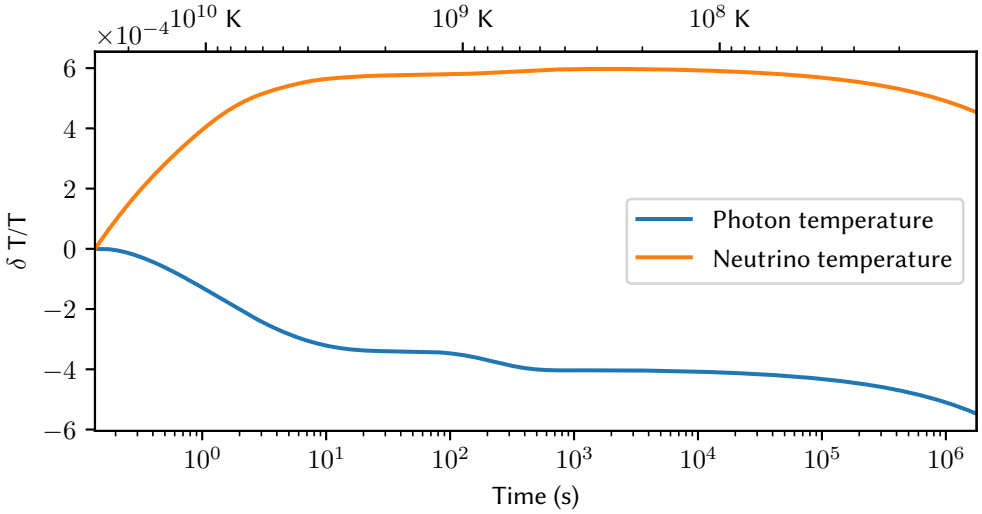

FIGURE 3.9: Relative deviation of temperatures as calculated by this code and AlterBBN. Positive values signify higher AlterBBN temperatures compared to this code.

the relation $T_\nu \propto a^{-1}$ holds exactly. This allows the baryon number density to be determined by $n_b = C \cdot T_\nu^3$ with the constant C being set by requiring $\eta =$ 6.1e-10 at late times.

	$Y_p \times 10$	^{2}H×10^5	^{3}He×10^5	^{7}Li ×10^{10}	^{6}Li ×10^{14}	^{7}Be ×10^{10}
100 MeV	2.470	2.532	1.040	4.712	0.750	4.411
2.3 MeV	2.472	2.536	1.040	4.706	0.752	4.404
This work using AlterBBN T_γ & T_ν	2.473	2.540	1.041	4.699	0.754	4.398
AlterBBN	2.474	2.467	1.034	5.363	1.087	5.075
+/−	0.003	0.038	0.016	0.352	1.085	0.343

TABLE 3.3: Comparison of final abundances for various background parameters. Showing results of this network using early and late instant neutrino decoupling, as well as the AlterBBN background which accounts for incomplete decoupling. The last row shows result from the AlterBBN background using their own abundance calculations.

The result of using the background parameters of AlterBBN are displayed on Table 3.3. Though somewhat obscured by the lack of significant digits, relative change caused by using the AlterBBN background is equal to 90% of the change caused by changing the timing of instant neutrino decoupling. This is due to the increase in T_ν/T_γ predicted by full incomplete decoupling, being 1.9 times greater than what is achieved by simply delaying instant decoupling. ^{4}He however only increases by 68% of that caused by delayed decoupling. This is due to ^{4}He being governed by the $p \leftrightharpoons n$ reactions, which take place while T_ν/T_γ is still increasing. This supports the previous assumption, that the only major difference between the cosmological calculation of AlterBBN and this code, is their inclusion of incomplete neutrino decoupling.

3.2.2 Reaction network

Since the difference in background introduces minimal abundance corrections, the discrepancy between the AlterBBN results and mine must unsurprisingly be due to differences in the reaction network. To see where these differences are we can plot the relative difference between abundances as they evolve during BBN, displayed on figure 3.10. Staring with the lightest nuclei, we see the small difference in neutron

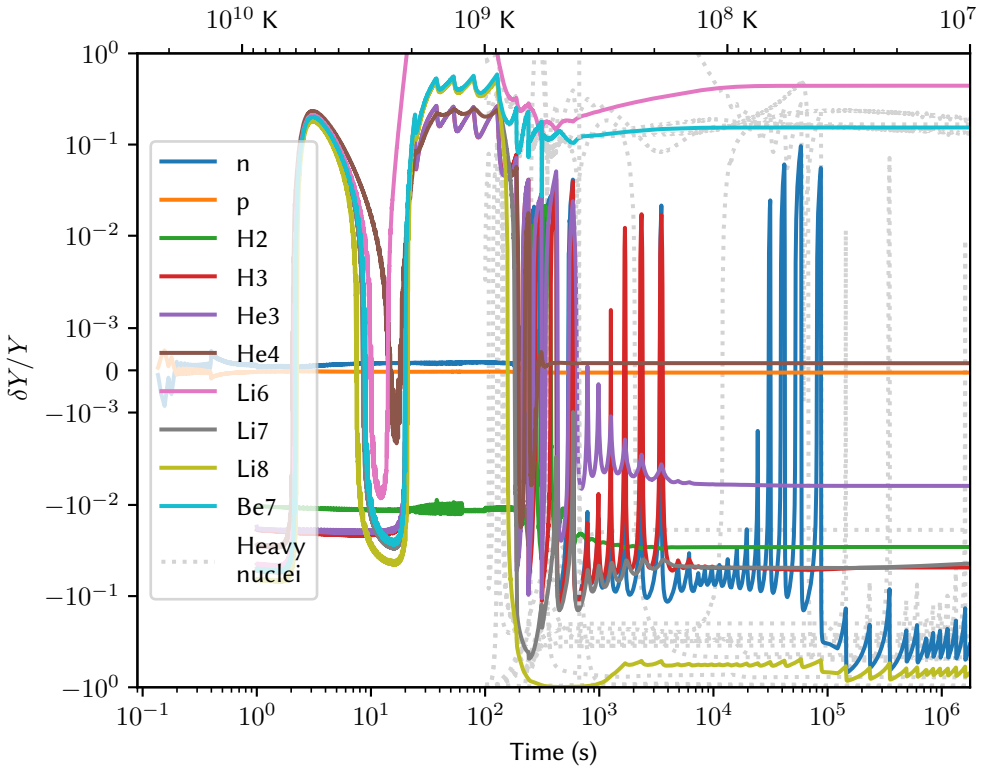

FIGURE 3.10: Relative deviation on abundances between this code and AlterBBN, during the various stages of BBN. To rule out cosmological differences, the AlterBBN background parameters are used for both calculations. Plot is linear in the region $\pm 10^{-3}$ and logarithmic outside.

proton ratio, and how this despite everything else, winds up resulting in an almost identical difference in Y_p. However, the most striking feature are the periodic spikes in relative abundance, affecting almost every single nuclei. This jaggedness originates in AlterBBN, and is caused by their implementation of certain reaction rates. As described in section 2.3, I use smooth fits of experimental data to obtain appropriate values for the reaction rates at any temperature. With every one of these rates stemming from the most recent snapshot of the REACLIB database[12] available in pynucastro[21]. AlterBBN on the other hand uses a manually curated list of reaction rates, with a myriad of different sources and implementations. A few of these rates are tabulated, and to obtain values between the tabulated temperature steps, AlterBBN simply uses nearest neighbor interpolation. This is hard coded as a series of consecutive else/if statements, which return the value of the reaction rate in discreet steps according to the nearest tabulated value. The spikes happen

whenever these rates assume a new value. For as an example AlterBBN uses a tabulated $^2H + p \rightarrow {}^3He$ rate from Coc et al. [13], which is responsible for the small early spikes in ^{3}He, and other nuclei that depend on its abundance. This can be confirmed by noting that the early spikes peak at 1.875, 1.625, 1.375, and 1.125 GK, which happen to be the exact midpoints between the tabulated values which are at 2, 1.75, 1.50, 1.25, and 1 GK.

Another difference is the relative increase and subsequent drop in ^{4}He abundances, which takes place between 2 and 20 seconds. This is caused by the $^3He + n \rightarrow {}^4He$ rate. Here AlterBBN uses a linear approximation for the rate, which stems from the original Wagoner code[5]. Though inaccurate, this reaction doesn't actually have a significant impact on final abundances since it only dominates ^{4}He production at very early times.

This leaves the main outliers, namely ^{7}Li and thereby ^{7}Be. The primary reactions responsible for creating and destroying ^{7}Li are $^3H + {}^4He \rightarrow {}^7Li$ and $^7Li + p \rightarrow 2{}^4He$, with ^{7}Be being governed by $^3He + {}^4He \rightarrow {}^7Be$ and $^7Be + n \rightarrow {}^7Li + p$. Compared to these, all other reactions are completely insignificant, which can be seen on figs. A.1 to A.4. For each of these four reactions a different rate is used by AlterBBN and my network.

Modifying the Network with AlterBBN rates

Due to the modular nature of my reaction network it is quite easy to simply swap the relevant reaction rates for those used by AlterBBN. Using the four ^{7}Li and ^{7}Be rates from AlterBBN as well as the previously mentioned $^3He + n \rightarrow {}^4He$ rate, a new set of final abundances can be obtained, table 3.4. As expected only the abundances of ^{7}Li

	$Y_p \times 10$	$^2H \times 10^5$	$^3He \times 10^5$	$^7Li \times 10^{10}$	$^6Li \times 10^{14}$	$^7Be \times 10^{10}$
Default rates	2.473	2.540	1.041	4.699	0.754	4.398
Rates from AlterBBN	2.473	2.540	1.041	5.133	0.754	4.837
AlterBBN	2.474	2.467	1.034	5.363	1.087	5.075
+/−	0.003	0.038	0.016	0.352	1.085	0.343

TABLE 3.4: Final abundances for the default network, the network using select AlterBBN rates, and the results from AlterBBN.

and ^{7}Be are affected, since the total abundances of light nuclei involved in the four reactions are much higher. Though the modified rates bring ^{7}Li and ^{7}Be abundances within the estimated uncertainty of AlterBBN, they still deviate significantly. To explain this figure 3.10 can be recreated using the modified reaction network.

Furthermore, the "new" $^3He + n \rightarrow {}^4He$ rate doesn't affect the final abundances.

The abundances still deviate from that of AlterBBN, which is

Using the major ^{7}Li and ^{7}Be rates from AlterBBN, we get updated final abundance

I recreate figure 3.10 resulting in figure 3.11. Looking at the early abundances we confirm that the initial difference in light nuclei abundance was indeed caused by the $^3He + n \rightarrow {}^4He$ rate. For the

Comparing the swapping out the

AlterBBN uses a different rate for each of these which

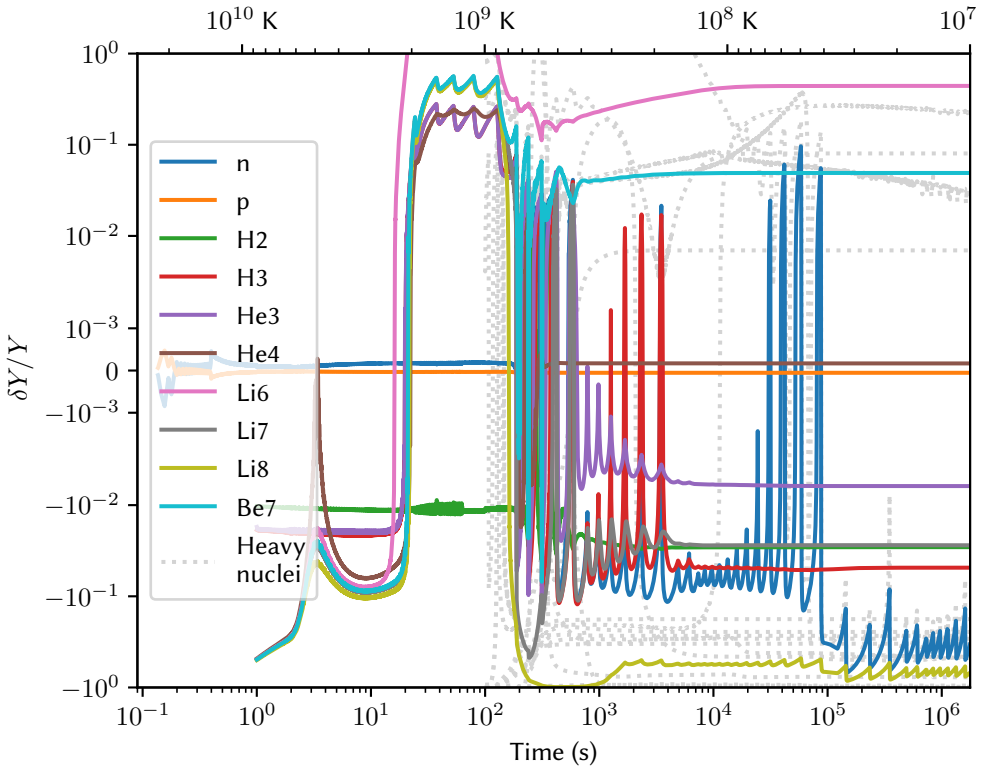

FIGURE 3.11: Same as fig. 3.10, but with the network using the same rates as AlterBBN for the reactions $^3\mathrm{He} + n \rightarrow {}^4\mathrm{He}$, $^7\mathrm{Li}$ are $^3\mathrm{H} + {}^4\mathrm{He} \rightarrow {}^7\mathrm{Li}$, $^7\mathrm{Li} + p \rightarrow 2{}^4\mathrm{He}$, $^3\mathrm{He} + {}^4\mathrm{He} \rightarrow {}^7\mathrm{Be}$, and $^7\mathrm{Be} + n \rightarrow {}^7\mathrm{Li} + p$.

3.3 Final abundances

3.4 Nuclear solutions to the Lithium problem?

Bibliography

[1] S. Chandrasekhar. *An Introduction to the Study of Stellar Structure*. First Edition. THE UNIVERSITY OF CHICAGO PRESS, 1939.

[2] R. A. Alpher, H. Bethe, and G. Gamow. "The Origin of Chemical Elements". In: *Phys. Rev.* 73 (7 Apr. 1948), pp. 803–804.

[3] P. J. E. Peebles. "Primordial Helium Abundance and the Primordial Fireball. II". In: *The Astrophysical Journal* 146 (Nov. 1966), p. 542.

[4] Robert V. Wagoner, William A. Fowler, and F. Hoyle. "On the Synthesis of Elements at Very High Temperatures". In: *The Astrophysical Journal* 148 (Apr. 1967), p. 3.

[5] Robert V. Wagoner. "Synthesis of the Elements Within Objects Exploding from Very High Temperatures". In: *The Astrophysical Journal Supplement* 18 (June 1969), p. 247.

[6] Robert Wagoner. "Big-Bang Nucleosynthesis Revisited". In: *The Astrophysical Journal* 179 (Dec. 1972), pp. 343–360.

[7] Lawrence Kawano. "Let's go: Early universe. 2. Primordial nucleosynthesis: The Computer way". In: (Jan. 1992).

[8] E. Kolb and M. Turner. *The Early Universe*. Frontiers in physics. Avalon Publishing, 1994.

[9] Steen Hannestad and Jes Madsen. "Neutrino decoupling in the early universe". In: *Phys. Rev. D* 52 (1995), pp. 1764–1769.

[10] B. Ryden. *Introduction to cosmology*. Second Edition. Cambridge University Press, 2002.

[11] P D Serpico et al. "Nuclear reaction network for primordial nucleosynthesis: a detailed analysis of rates, uncertainties and light nuclei yields". In: *Journal of Cosmology and Astroparticle Physics* 2004.12 (Dec. 2004), pp. 010–010.

[12] Richard H. Cyburt et al. "The JINA REACLIB Database: Its Recent Updates and Impact on Type-I X-ray Bursts". In: *The Astrophysical Journal Supplement* 189.1 (July 2010), pp. 240–252.

[13] Alain Coc et al. "New reaction rates for improved primordial D/H calculation and the cosmic evolution of deuterium". In: *Phys. Rev. D* 92 (12 Dec. 2015), p. 123526.

[14] Pablo F. de Salas and Sergio Pastor. “Relic neutrino decoupling with flavour oscillations revisited”. In: *Journal of Cosmology and Astroparticle Physics* 2016.07 (July 2016), pp. 051–051.

[15] Cyril Pitrou, Alain Coc, Jean-Philippe Uzan, and Elisabeth Vangioni. “Precision big bang nucleosynthesis with improved Helium-4 predictions”. In: *Submitted to Phys. Rept.* (2018).

[16] A. Arbey, J. Auffinger, K. P. Hickerson, and E. S. Jenssen. *AlterBBN v2: A public code for calculating Big-Bang nucleosynthesis constraints in alternative cosmologies*. 2019.

[17] Planck Collaboration et al. “Planck 2018 results. VI. Cosmological parameters”. In: *Astronomy and Astrophysics* 641, A6 (Sept. 2020), A6.

[18] Pauli Virtanen et al. “SciPy 1.0: Fundamental Algorithms for Scientific Computing in Python”. In: *Nature Methods* 17 (2020), pp. 261–272.

[19] Charlie Sharpe, Geraint F. Lewis, and Luke A. Barnes. *Big Bang Nucleosynthesis Initial Conditions: Revisiting Wagoner et al. (1967)*. 2021.

[20] S. Gariazzo, P. F. de Salas, O. Pisanti, and R. Consiglio. “PArthENoPE revolutions”. In: *Computer Physics Communications* 271 (Feb. 2022), p. 108205.

[21] Alexander I. Smith et al. “pynucastro: A Python Library for Nuclear Astrophysics”. In: *The Astrophysical Journal* 947.2 (Apr. 2023), p. 65.

[22] *NIST Digital Library of Mathematical Functions*. `https://dlmf.nist.gov/`, Release 1.1.11 of 2023-09-15. F. W. J. Olver, A. B. Olde Daalhuis, D. W. Lozier, B. I. Schneider, R. F. Boisvert, C. W. Clark, B. R. Miller, B. V. Saunders, H. S. Cohl, and M. A. McClain, eds.

Appendix A

Additional plots

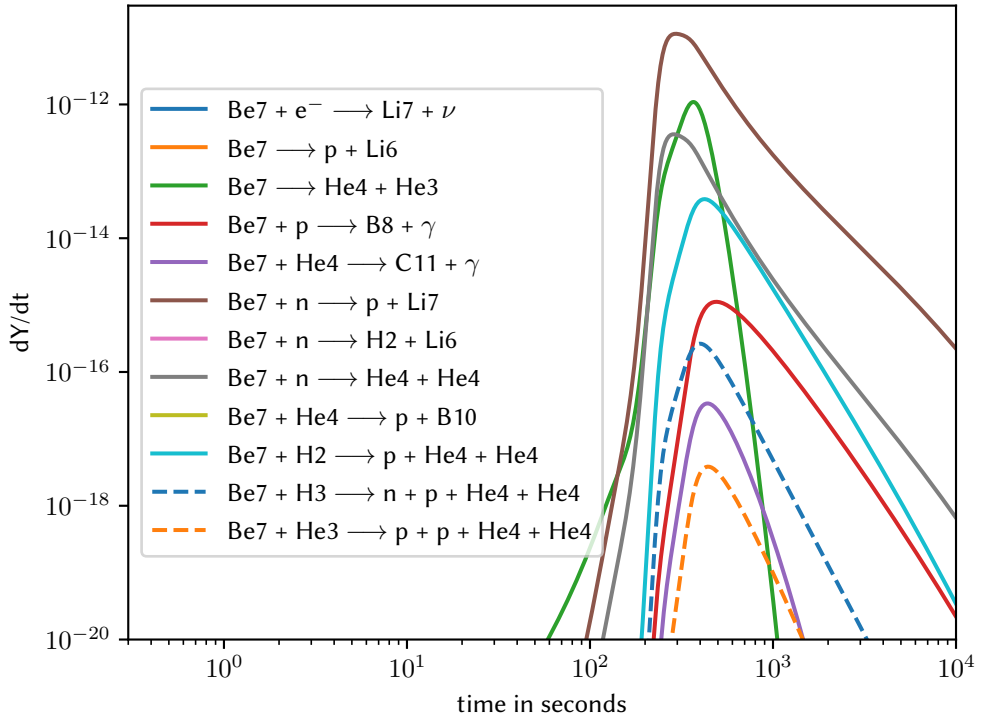

Figure A.1: Strength of different ^{7} Be destruction rates.

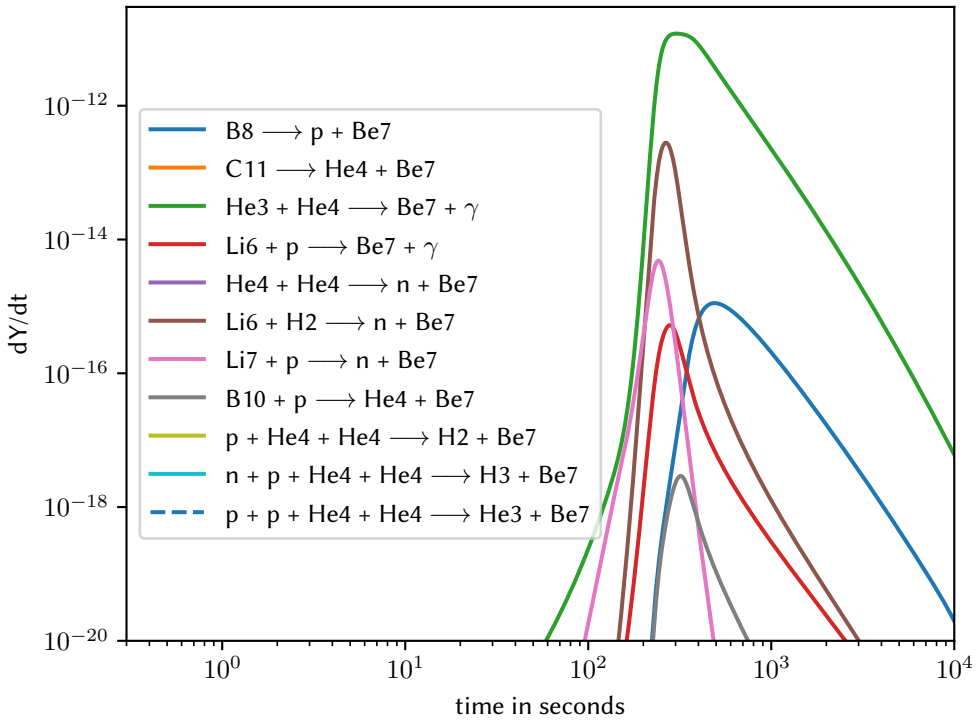

FIGURE A.2: Strength of different ^{7} Be creation rates.

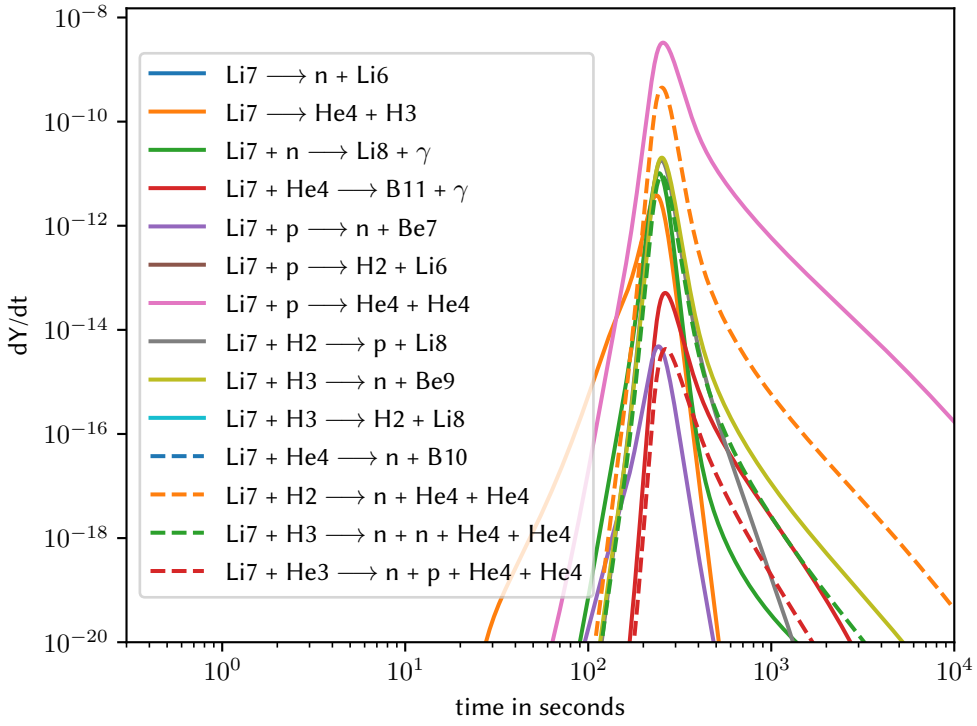

FIGURE A.3: Strength of different ^{7} Li destruction rates.

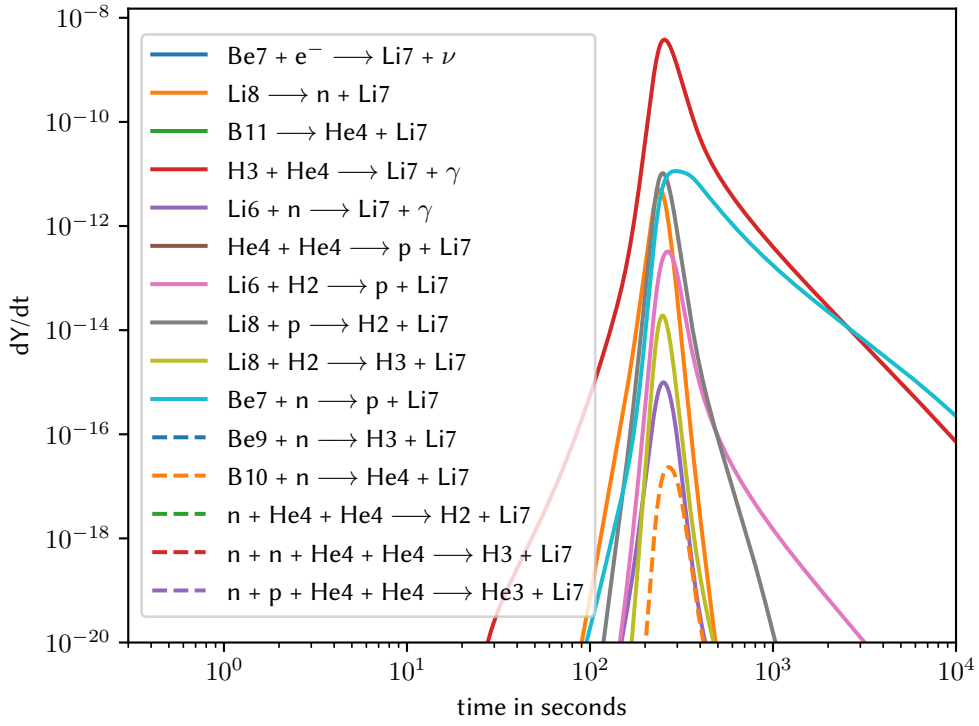

FIGURE A.4: Strength of different ^{7} Li creation rates.